

Distribution functions for clusters of galaxies from N-body simulations

Priyamvada Natarajan¹, Jens Hjorth¹ and Eelco van Kampen²

¹*Institute of Astronomy, Madingley Road, Cambridge CB3 0HA*

²*Royal Observatory, Blackford Hill, Edinburgh EH9 3HJ*

26 July 2021

ABSTRACT

We present the results of an attempt to adapt the distribution function formalism to characterize large-scale structures like clusters of galaxies that form in a cosmological N-body simulation. While galaxy clusters are systems that are not strictly in equilibrium, we show that their evolution can nevertheless be studied using a physically motivated extension of the language of equilibrium stellar dynamics. Restricting our analysis to the virialized region, a prescription to limit the accessible phase-space is presented, which permits the construction of both the isotropic and the anisotropic distribution functions $f(\mathcal{E})$ and $f(\mathcal{E}, L)$. The method is applied to models extracted from a catalogue of simulated clusters. Clusters evolved in open and flat background cosmologies are followed during the course of their evolution, and are found to transit through a sequence of what we define as ‘quasi-equilibrium’ states. An interesting feature is that the computed $f(\mathcal{E})$ is well fit by an exponential form. We conclude that the dynamical evolution of a cluster, undergoing relaxation punctuated by interactions and violent mergers with consequent energy-exchange, can be studied both in a qualitative and quantitative fashion by following the time evolution of $f(\mathcal{E})$.

Key words: celestial mechanics, stellar dynamics – cosmology: theory – dark matter – galaxies: clusters: general

1 INTRODUCTION AND MOTIVATION

In this paper we present the results of an attempt to construct distribution functions for clusters of galaxies that form in N-body simulations. To permit the description of systems like clusters that are continually evolving at the present epoch we propose a possible extension of the distribution function formalism of equilibrium stellar dynamics. The prescription developed is applied to simulated clusters for which the isotropic and anisotropic distribution functions are computed. We then use the time evolution of the distribution function to get an insight into the details of the relaxation process and energy exchange in clusters.

The motivation for this work is twofold: (i) to develop a mathematical formalism to characterize the dynamical evolution of ‘stellar’ systems that are marginally out of equilibrium, which can be applied to numerical cluster models and (ii) to gain insight into the dynamical evolution and properties of clusters in general with as special emphasis on the origin of density profiles and the use of clusters as cosmological probes.

Previous studies that are relevant to our work have been done in three somewhat distinct contexts: (i) studies of the

dynamical state of clusters formed in N-body simulations, (ii) studies of the formation and evolution of elliptical galaxies in an attempt to understand the physical origin of the universal $R^{1/4}$ law and (iii) the evolution of stellar systems studied in phase space.

Given the standard paradigm of Cold Dark Matter (CDM) dominated hierarchical structure formation scenarios, the formation, internal structure and evolution of dark halos and density profiles has been studied in detail for a range of initial input power spectra evolved in a slew of background cosmological models (Goldreich 1984; Hoffman & Shaham 1985; West, Dekel, & Oemler 1987; Crone, Evrard, & Richstone 1994; Richstone, Loeb, & Turner 1992; Cen, Gnedin, & Ostriker 1993; Klypin et al. 1993; Cen 1994; Navarro & White 1994; Dodds 1995). A ‘universal density profile’ has been found to be a good fit over a two-decade range of scales for dark halos that form in N-body realizations of the cosmological model (Navarro, Frenk, & White 1996; White 1996). These authors and several other groups (Cole & Lacey 1996; Tormen, Bouchet, & White 1996) find that for a range of cluster-halo shapes, sizes and other bulk properties, the profile depends primarily on the epoch of formation and only rather weakly on the details of the cos-

mological context and the initial power spectrum of fluctuations. Navarro, Frenk, & White (1996) find that their spherically averaged density profiles can be fit by scaling a ‘universal’ profile (henceforth referred to as the NFW profile) which goes as $\rho \propto r^{-1}$ at small radii and steepens to $\rho \propto r^{-3}$ at large radii. Subsequently, Cole & Lacey (1996) on examining the internal structure of dark matter halos formed in scale-free hierarchical models for a range of initial power spectra, also find that the density profile is well-fit by both the NFW profile and the analytic Hernquist (1990) profile which falls off as $\rho \propto r^{-4}$ at large radii. Part of the aim of the present investigation is to explore the interplay between the initial conditions and subsequent relaxation processes in clusters and to understand the possible physical origin of these density profiles.

This approach is somewhat analogous to the detailed studies of the origin of the $R^{1/4}$ law in elliptical galaxies (van Albada 1982; Carlberg, Lake, & Norman 1986; Londrillo, Messina, & Stiavelli 1991; Hjorth & Madsen 1991). Moving over to the analogy with the formation of elliptical galaxies, we briefly review some scenarios that have been put forward to understand the observed universal $R^{1/4}$ profile. The physical system in this case essentially consists of stellar orbits in a potential which deepens during the course of evolution via violent relaxation that occurs as a consequence of strong collective potential fluctuations (Lynden-Bell 1967). During the course of evolution following the violent phase, any remaining positive energy particles slowly diffuse out and eventually leave the system. In the case where the resultant stellar system has a deep potential well the $R^{1/4}$ surface-brightness profile arises as a natural consequence (Hjorth & Madsen 1991). Such a final configuration can be produced from a cold dissipationless collapse scenario leading to stellar orbits that are preferentially radially anisotropic as well as from warmer initial conditions with dissipation.

While universality intuitively suggests wiping out of the memory of initial conditions and similarities in the post-collapse evolution, Londrillo, Messina, & Stiavelli (1991) conclude from their study of dissipationless galaxy formation that the phase-space properties of the final equilibrium state do in fact depend strongly on the details of the initial conditions. They find that the relaxation to an $R^{1/4}$ profile is characterized by two phases: (i) an early phase dominated by strong potential and density fluctuations in the central region which results in a core-halo structure and a long tail in both the density and energy distribution and (ii) a longer-lived later phase wherein the system evolves mainly due to the effect of small-scale diffusion which smoothes the connection between the core and the halo populations. Some memory of the early phase is retained, since the fluctuating forces and the compact core necessary to diffuse the low angular momentum orbits in the later phase are necessarily remnants of the initial collapse dynamics; i.e. the region of phase space that is available for diffusion into for the system during the late phase is delineated during the early phase. Also in dissipational scenarios (Barnes 1996) which are expected to introduce irreversibility, especially during mergers, some memory of the initial conditions seems to be retained.

Finally, we place this work in the context of studies of the evolution of stellar systems in phase space. The structure of phase space and its accessibility for $R^{1/4}$ galaxies was explored by Binney (1982) who found that the distribution of

the number of stars of a given energy is approximated rather well by an exponential formula. It was argued that if elliptical galaxies formed via dissipationless processes, the exponential form found at late times for the distribution function was probably set up during the epoch of formation, yielding a scale-free form for the density profile. Therefore, the phase space corresponding to the observed surface brightness profiles of elliptical galaxies are consistent with having been demarcated during the initial collapse of a density fluctuation that subsequently gives rise to the galaxy. In another study, Hernquist, Spergel, & Heyl (1993) attempted to quantify the importance of mergers in the origin and structure of early-type galaxies by exploring the phase-space properties of merger remnants and comparing them to simple models of elliptical galaxies.

In a more recent analysis, Voglis (1994) presents an analytic model fit to the distribution function of a nearly spherical, anisotropic galaxy-scale system. Starting with cosmologically consistent initial conditions, he finds a dichotomy of states, a core population dominated by low angular-momentum tightly bound particles and a less bound halo population. The energy distribution of the core population is nearly isothermal whereas the halo population consists of particles on radial orbits with correlated energy and angular momentum. Following the time evolution of a radius containing a specific fraction of the mass, he finds that the radial oscillations decay quickly after collapse preceding the onset of relaxation during which a new equilibrium is established.

Despite some essential physical differences between stellar systems and clusters, we synthesize the approaches described above and demonstrate that they can be adapted and successfully applied to the case of galaxy clusters that form in realizations of cosmological N-body simulations. Specifically, we develop in the present paper a framework that can be applied to characterizing what we shall define as *quasi-equilibrium evolution*. In Section 2 we outline our conceptual model of a cluster, review the equilibrium distribution function formalism and present our prescription to extend it to quasi-equilibrium. The details of the N-body simulations from which the cluster catalogs that we study were extracted are described in Section 3. In Section 4 we apply the method to the construction of $f(\mathcal{E})$ and $f(\mathcal{E}, L)$ for slices from the simulations. We present our results and summarize what can be learnt from a first set of diagnostics developed to describe the quasi-equilibrium evolutionary states of the cluster in Section 5.

2 THE DISTRIBUTION FUNCTION FORMALISM

2.1 Characterizing a cluster

A cluster is a composite system with diverse components: collisionless dark-matter particles, collisional baryonic gas and bound stellar systems (the galaxies). The rudimentary physical picture of the cluster that we find useful, is one of a system with two natural length scales delineated by the dynamics: the virial radius r_{vir} , defined to be the radius enclosing an overdensity of ≈ 180 times the critical density, which is motivated by the collapse of the simple spherical

top-hat model (Peebles 1980) and the turnaround radius r_{ta} , defined to be the radius at which the cluster separates from the general cosmological expansion (envelope with zero relative velocity). There is on-going infall inward of r_{ta} , and therefore the system can never really be treated as one evolving in isolation.

It is instructive to clarify at this juncture some of the terms and their definitions that will be employed in our analysis to describe the dynamical state of the system. A *virialized* system is one for which the virial theorem holds ($d^2 I_{ij}/dt^2 = 0$; where I_{ij} is the moment of inertia tensor) and therefore there exist no systematic motions, neither expansion nor contraction; a *stationary* system is one for which there is no time variation of the distribution function f , i.e. $\partial f/\partial t = 0$, and a *relaxed system* is one for which memory of the initial conditions in phase-space has been erased. For a cluster-scale collisionless system, two-body relaxation processes are unimportant since the time-scale relevant for two-body processes far exceeds the dynamical time, although in the case of a simulated cluster, there arise some purely numerical two-body effects which we discuss in more detail in Section 3. While collective energy exchange processes might occur during the course of dynamical evolution, they might not always lead to a relaxed final state and also a virialized system need not be relaxed. This is so because virialization is defined in terms of the kinetic and potential energies of a specific configuration of the system at a given epoch, while relaxation requires physical processes that affect the evolution to be taken into account and is hence a statement about the integrated dynamical history.

In this study we focus on the collisionless component. We define a collisionless equilibrium system to be one that is virialized, stationary and relaxed with no on-going energy exchange. Clearly, this is not the case for a cluster of galaxies, wherein departures from equilibrium necessarily occur due to the existence of an infall region and departure from stationarity which is a consequence of fluctuations induced in the potential in response to mergers and secondary infall. Nevertheless, there does seem to exist a virialized central region and observed clusters seem not to be far from equilibrium as inferred from their ‘measured’ density profiles and velocity dispersions. Therefore, the need arises to develop a phase-space description that can incorporate small departures from equilibrium, which we attempt below. To first approximation, we model a cluster in this treatment as a spherically symmetric and non-rotating system.

2.2 The equilibrium distribution function formalism

For a statistical description of a system with a large number of particles, it is convenient to define the distribution function (DF) (the phase-space mass density) $f(\mathbf{r}, \mathbf{v}, t)$. A given configuration of the system is then specified by $f(\mathbf{r}, \mathbf{v}, t) d^3 \mathbf{x} d^3 \mathbf{v}$ – the mass of particles having positions in the infinitesimal volume element $d^3 \mathbf{r}$, with velocities in the range $d^3 \mathbf{v}$ in the (\mathbf{r}, \mathbf{v}) phase space. The DF satisfies the Boltzmann equation,

$$\frac{df}{dt} = \frac{\partial f}{\partial t} + \mathbf{v} \cdot \nabla f - \nabla \Phi \cdot \frac{\partial f}{\partial \mathbf{v}} = C, \quad (1)$$

where df/dt is the total derivative along the exact trajectory of the particle moving in the force field $\nabla \Phi$ and C is the collisional term, which defines the changes in f due to collisions between particles. In conjunction with the Poisson equation,

$$\nabla^2 \Phi = 4\pi G \rho, \quad (2)$$

and the definition of the density profile,

$$\rho(\mathbf{r}, t) = \int f(\mathbf{r}, \mathbf{v}, t) d^3 \mathbf{v}, \quad (3)$$

equations (1), (2) and (3) constitute a complete set of self-consistent evolution equations that describe a self-gravitating system. For a stellar system that is strictly collisionless and gravitating, $C = 0$ in equation (1), the solutions to the above are the stationary states, and the particle trajectories are the ‘characteristics’. Additionally, while equation (2) is valid only for a self-gravitating system, the potential defined in equation (1) could also include the contribution from an external potential.

We review below some of the basic definitions that will be used throughout the paper; a more comprehensive treatment of the formalism can be found in Binney & Tremaine (1987). The notational conventions followed here are also as in Binney & Tremaine (1987) except for the introduction of the function h .

The binding energy per unit mass \mathcal{E} is defined as,

$$\mathcal{E} = \Psi(r) - \frac{v^2}{2}, \quad (4)$$

and the angular momentum per unit mass L is given by,

$$L = |\mathbf{r} \times \mathbf{v}|. \quad (5)$$

The DF for a spherically symmetric, non-rotating stellar system can only depend on these two quantities. Dependence on both \mathcal{E} and L gives rise to an anisotropic velocity distribution whereas dependence on \mathcal{E} only yields an isotropic distribution of velocities. The differential energy distribution $(dM(\mathcal{E})/d\mathcal{E}) d\mathcal{E}$ is the total mass of the system with binding energy within $[\mathcal{E}, \mathcal{E} + d\mathcal{E}]$ which is then explicitly defined to be,

$$h(\mathcal{E}) d\mathcal{E} \equiv \frac{dM(\mathcal{E})}{d\mathcal{E}} d\mathcal{E} = \int_{\Delta V(\mathcal{E})} f(\mathcal{E}) d^3 \mathbf{r} d^3 \mathbf{v}, \quad (6)$$

integrated over the volume element $\Delta V(\mathcal{E})$ in phase-space with energy in the specified range $[\mathcal{E}, \mathcal{E} + d\mathcal{E}]$. Since we are dealing with spherically symmetric systems we can write this integral in terms of r and v . Furthermore, we can take $f(\mathcal{E})$ out of the integral and use eq. (4) to arrive at:

$$h(\mathcal{E}) d\mathcal{E} = 16\pi^2 f(\mathcal{E}) d\mathcal{E} \int_0^{r_m(\mathcal{E})} r^2 dr \sqrt{2(\Psi(r) - \mathcal{E})}. \quad (7)$$

This can be written as

$$h(\mathcal{E}) d\mathcal{E} = f(\mathcal{E}) g(\mathcal{E}) d\mathcal{E}, \quad (8)$$

where $g(\mathcal{E})$ the density of available states in phase space of energy \mathcal{E} ,

$$g(\mathcal{E}) \equiv 16\pi^2 \int_0^{r_m(\mathcal{E})} \sqrt{2(\Psi(r) - \mathcal{E})} r^2 dr. \quad (9)$$

This integral is strictly defined only for $\Psi(r) \geq \mathcal{E}$. Here $r_m(\mathcal{E})$ is defined to be the radius where $\Psi(r_m) = \mathcal{E}$. Thus,

we obtain an operational definition for $f(\mathcal{E})$,

$$f(\mathcal{E}) = \frac{h(\mathcal{E})}{g(\mathcal{E})}. \quad (10)$$

Given a potential $\Psi(r)$, both $h(\mathcal{E})$ and $g(\mathcal{E})$ are well-defined for stellar systems in equilibrium. We use the definition in equation (9) to construct the DF in our analysis. The DF could alternatively be derived and hence constructed by either explicitly counting available and energetically accessible cells in phase space or from the density profile of the system $\rho(r)$ using an inversion method devised by Eddington (1916). Quoting the result of Eddington's inversion formula from Binney (1982),

$$f(\mathcal{E}) = \frac{1}{\sqrt{8\pi^2}} \int_0^\mathcal{E} \frac{d^2\rho}{d\Psi^2} \frac{d\Psi}{\sqrt{\Psi - \mathcal{E}}} + \frac{1}{\sqrt{\mathcal{E}}} \frac{d\rho}{d\Psi}, \quad (11)$$

$$\frac{d^2\rho}{d\Psi^2} = \left(\frac{r^2}{GM} \right)^2 \left[\frac{d^2\rho}{dr^2} + \frac{d\rho}{dr} \left(\frac{2}{r} - \frac{4\pi\rho r^2}{M(r)} \right) \right] \quad (12)$$

where $M(r)$ is the total mass enclosed within radius r of the system.

For a spherically symmetric system with an anisotropic velocity distribution, the DF $f(\mathcal{E}, L)$ is analogously defined to be,

$$f(\mathcal{E}, L) = \frac{h(\mathcal{E}, L)}{g(\mathcal{E}, L)}. \quad (13)$$

The density of states in phase-space $g(\mathcal{E}, L)$ is now a hypersurface of energy \mathcal{E} and angular momentum L . Furthermore,

$$g(\mathcal{E}, L) = 8\pi^2 L T_r(\mathcal{E}, L), \quad (14)$$

where T_r is the radial period defined as,

$$T_r(\mathcal{E}, L) = \int_{r_1}^{r_2} \frac{dr}{\sqrt{2(\Psi(r) - \mathcal{E}) - \frac{L^2}{r^2}}}, \quad (15)$$

the range of integration being from the pericenter of the orbit, r_1 , to the apocenter, r_2 . The radial period $T_r(\mathcal{E}, L)$ is generally evaluated numerically, but an approximately analytic expression can be obtained for a few special choices of the potential; one of them being the isochrone potential, for which the following simple expression holds,

$$T_r(\mathcal{E}, L) = \frac{2\pi GM}{(2\mathcal{E})^{3/2}}. \quad (16)$$

Furthermore, $T_r(\mathcal{E}, L)$ has been demonstrated to be almost independent of L for different potentials (isochrone and Keplerian in particular) by Voglis (1994) and Lynden-Bell (1996).

2.3 Adapting the DF formalism to quasi-equilibrium

The equilibrium formalism outlined above does not strictly apply to clusters of galaxies as these systems are constantly evolving. Additionally, the equilibrium formalism as currently posed cannot accommodate the existence of positive energy particles that are sometimes observed in numerical cluster simulations (see plots in Section 5). On the other hand, it appears to be sensible to attempt using the equilibrium formalism as a guide to probe the non-equilibrium

domain. Indeed, most studies of the dynamics of clusters of galaxies implicitly assume that an equilibrium description is an adequate starting point.

Below we first describe the inherent limitations that such an approach is necessarily subject to, but we then use precisely these restrictions to formulate a physically motivated and self-consistent extension of the equilibrium formalism. The key to the extension arises from the recognition of the important distinguishing features in the case of clusters: the finite time available for evolution and the spatial extent of a cluster.

Examining the relevant time-scales: firstly, the typical time that it takes for a cluster to be virialized out to the Abell radius is of the order of the Hubble time which in itself precludes the cluster from reaching an equilibrium configuration. Secondly, the disturbances from continuous infall and the more violent interactions constantly drive the system away from equilibrium whereas the collective energy exchange processes tend to drive the system toward equilibrium. The fact that the characteristic time-scale on which the collective energy exchange process operate is relatively short means that the system is capable of quickly recouping from or adapting to a disturbance. Thus, it is possible that the system might come close to equilibrium fairly quickly after such events. In other words, it may be possible to decouple the system into two components: a fast component and a slowly evolving component, akin to the adiabatic approximation. We may therefore view the system as evolving from one *quasi-equilibrium* state to another on a time scale that is roughly the 'disturbance time scale'.

Having thus argued that the system might frequently be close to a quasi-equilibrium state, we need to delineate more precisely the specific region to which such a treatment is most suitably applicable. Since the use of the equilibrium formalism necessarily requires the system to be virialized, a natural choice would be to study a typical virialized region; clearly, the infall region cannot be studied via this approach. Also, once a radially infalling particle has entered the virialized region its kinetic energy gets distributed to other particles and it is more likely to get bound inside the virialized region rather than leave the system. Moreover, even the few particles that are capable of leaving the region are more than balanced in the net by the infalling ones.

In summary, the finite time and extent arguments coupled with the expected short relaxation time scale encourage us to develop the notion of quasi-equilibrium states further. However, the eventual usefulness and indeed validity of the approach should be judged not on these arguments alone but on the results presented in Sections 4 and 5. We reiterate that our proposed adapted equilibrium formalism is only applicable to a restricted region in phase space.

There have been several previous studies that have attempted to limit the available phase space for elliptical galaxies (Stiavelli & Bertin 1987; Tremaine 1987; Merritt, Tremaine, & Johnstone 1989). For instance, Spergel & Hernquist (1992) suggested a prescription to limit the macroscopic states that are accessible to individual particles in a collisionless system approaching equilibrium by approximating violent dynamical processes en-route to relaxation as a sequence of discrete scattering events. They also introduced a monotonically increasing non-equilibrium entropy by imposing additional constraints on the available phase-space.

In our approach we make no *a priori* assumptions about the nature of energy-exchange processes and do not attempt to define any generalized entropy for the system. Rather we shall argue that it is the usual definitions (8) and (13) of $g(\mathcal{E})$ and $g(\mathcal{E}, L)$ that need to be modified in a consistent fashion to enable the description of systems evolving marginally away from equilibrium.

2.3.1 Computing $g(\mathcal{E})$ for non-equilibrium systems

As described in Section 2.2, the phase-space density $g(\mathcal{E})$ is valid only for negative energies (positive \mathcal{E} , i.e. strictly bound particles in an equilibrium system), and diverges for $\mathcal{E} \rightarrow 0$ due to the blowing up of the volume element in physical space. For instance, consider a potential $\Psi(r)$ with a radial dependence such that,

$$\Psi(r) = r^{-\alpha}; \quad 0 < \alpha \leq 1. \quad (17)$$

In this case $r_m(\mathcal{E}) \sim \mathcal{E}^{-\alpha}$ and so $g(\mathcal{E})$ diverges as \mathcal{E}^η for $\eta = \alpha^2/2 - 3\alpha$, i.e., $-5/2 \leq \eta < 0$. Requiring $f(\mathcal{E})$ to be finite at the escape energy and the mass to be finite simultaneously implies that $\eta > -1$, in turn restricting $0 < \alpha < 3 - \sqrt{5}$ which for the self-gravitating case ($\alpha = 1$) means that the asymptotic behavior of $g(\mathcal{E})$ cannot be compensated by a similar divergence of $h(\mathcal{E})$. Furthermore, $g(\mathcal{E})$ is infinite for all $\mathcal{E} \leq 0$, as the accessible phase-space is infinite for these energies. As discussed above, we propose to limit the accessible phase-space due to the finite time available. We do this in practice by truncating $g(\mathcal{E})$ at a fixed scale r_{\max} . As we show below, this will remove the divergence and render $g(\mathcal{E})$ well-behaved for all \mathcal{E} .

Physically, such a truncation amounts to the assumption that for most of the bound particles that constitute the system, the finite time elapsed since the initial collapse necessarily implies that the probability of occupation of states falls off steeply beyond a fiducial volume in phase space which is dictated by the threshold distance that a particle with typical velocities can traverse in the available time interval. Energy-exchange and hence marginal departures from equilibrium of the cluster arise both from the existence of the extended infall region as well as due to the occurrence of frequent mergers and interactions as an integral part of the relaxation process. Since, in this analysis, we are primarily interested in probing and characterizing the evolution of the central regions and the relaxation effects therein, we choose to truncate the system at $r_{\max} = r_{180} = r_{\text{vir}}$, the radius within which the system is expected to be virialized, and is indeed found to be for several different power spectra (Cole & Lacey 1996). This prescription is independent of the functional form for the potential and can in general be applied to any physically meaningful potential for a spherically symmetric system.

Specifically, consider a stellar system consisting of particles confined in a potential $\Psi(r)$, modelled explicitly as the Hernquist potential,

$$\Psi(r) = \frac{\Psi_0}{1 + \frac{r}{s}}. \quad (18)$$

In the equilibrium context, the limits of integration for $g(\mathcal{E})$ range from 0 to $r_m(\mathcal{E})$ defined to be the radius at which $\Psi(r_m) = \mathcal{E}$.

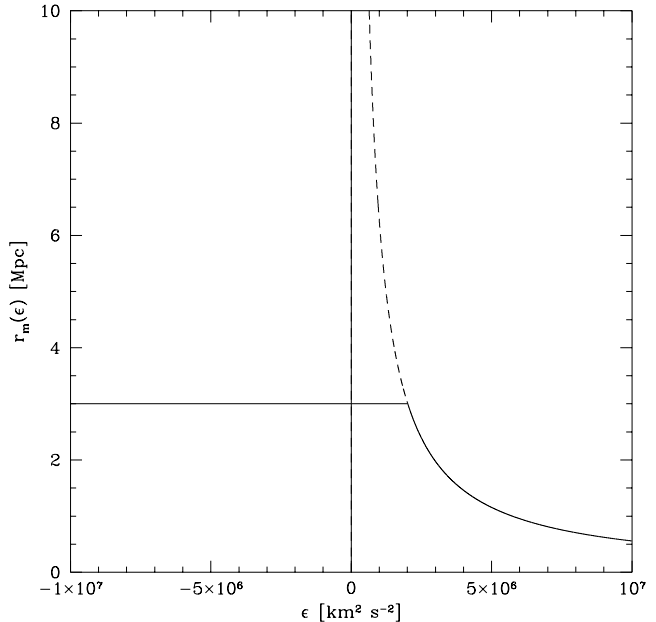


Figure 1. The prescription for truncation: we illustrate the prescription we have used to define r_{\max} , the truncation radius, for the Hernquist potential. The solid curve is our choice for r_{\max} , which now stands well-defined for all \mathcal{E} .

From the plot in Fig. 1, we see clearly that the phase-space volume element is ill-defined as $\mathcal{E} \rightarrow 0^+$. By setting r_{\max} as the maximal allowed value for $r_m(\mathcal{E})$ in eq. (8), i.e.,

$$r_m(\mathcal{E}) = \text{Min} \left[s \left(\frac{\Psi_0}{\mathcal{E}} - 1 \right), r_{\max} \right], \quad (19)$$

we truncate the system in physical space, which automatically translates into a restriction of available phase-space. In this way we recover a well-behaved $g(\mathcal{E})$ that is valid for all \mathcal{E} .

Thus, using only the assumption that the number of particles within the boundary r_{\max} is roughly constant, we modify the definition of $g(E)$ to allow for quasi-equilibrium states (including the temporary existence of positive energy particles). With this modification, most of the equilibrium formalism then automatically carries over for spherically symmetric systems.

2.3.2 Computing $g(\mathcal{E}, L)$ for non-equilibrium systems

The construction of $g(\mathcal{E}, L)$ is analogous to the above, but we now need to restrict a two-dimensional hypersurface. The key observation here is that in addition to the restriction in r_{\max} , the orbital structure needs to be constrained correspondingly in a consistent fashion. We proceed as follows, by first assuming that $g(\mathcal{E}, L)$ is separable,

$$g(\mathcal{E}, L) = L \tilde{g}(\mathcal{E}), \quad (20)$$

motivated by the functional form of the expression for $g(\mathcal{E}, L)$ (eq. 13), and the observation of Voglis (1994) that the radial period $T_r(\mathcal{E}, L)$ is only a weak function of L . A functional form for $\tilde{g}(\mathcal{E})$ can then be derived by integrating

$g(\mathcal{E}, L)$ over L :

$$g(\mathcal{E}) = \int_0^{L_{\max}} L \tilde{g}(\mathcal{E}) dL = \tilde{g}(\mathcal{E}) L_{\max}^2 / 2. \quad (21)$$

Therefore,

$$\tilde{g}(\mathcal{E}) = \frac{2g(\mathcal{E})}{L_{\max}^2}, \quad (22)$$

and

$$g(\mathcal{E}, L) = \frac{2g(\mathcal{E})L}{L_{\max}^2}, \quad (23)$$

where the expression is valid for all \mathcal{E} , provided L_{\max} is appropriately defined as the specific angular momentum per unit mass for a circular orbit of energy \mathcal{E} . Given the prescription for defining $r_m(\mathcal{E})$, the maximal allowed angular momentum for a particle is easily calculated once the circular velocity at a given radius in the potential is known. For the Hernquist potential one obtains,

$$L_{\max}(\mathcal{E}) = r_m^2(\mathcal{E}) \frac{\Psi_0 s}{(1 + \frac{r_m(\mathcal{E})}{s})}. \quad (24)$$

With the modified definitions of $g(\mathcal{E})$ and $g(\mathcal{E}, L)$ we have thus successfully adapted the equilibrium DF formalism for systems in quasi-equilibrium enabling the construction of both $f(\mathcal{E})$ and $f(\mathcal{E}, L)$.

3 NUMERICAL CLUSTER MODELS

3.1 Numerical methods

We briefly summarize the modelling of the clusters that we intend to study. Initial conditions for the cluster models are generated by means of the van de Weygaert & Bertschinger (1996) implementation of the Hoffman-Ribak method of constrained random fields (Hoffman & Ribak 1991) in order to form a specific cluster at the centre of the simulation sphere. Each cluster model is evolved from these constrained initial conditions by means of the Barnes & Hut 1989 treecode, supplemented with a galaxy formation algorithm (see van Kampen 1996 for details). During the evolution, galaxies are identified at several epochs and replaced by single ‘galaxy particles’ in order to ensure their survival, as numerical two-body disruption destroys almost all galaxies inside standard N-body cluster simulations (van Kampen 1995; Carlberg 1995). Two-component models consisting of distributions of dark-matter background particles and galaxy particles are thus produced. A direct match of the simulated galaxy distribution with the observed one sets the amplitude of the initial density fluctuation spectrum, and thus the present time in the models. The specific prescription used to define galaxies is necessarily somewhat arbitrary. However, we consider that it provides at least a crude representation of the influence galaxies have on the dark matter distribution. The implementation of alternate prescriptions to define ‘galaxies’ is unlikely to substantially modify the results presented here. In any case, for this paper we have examined only the distribution and dynamics of the dominant dark component.

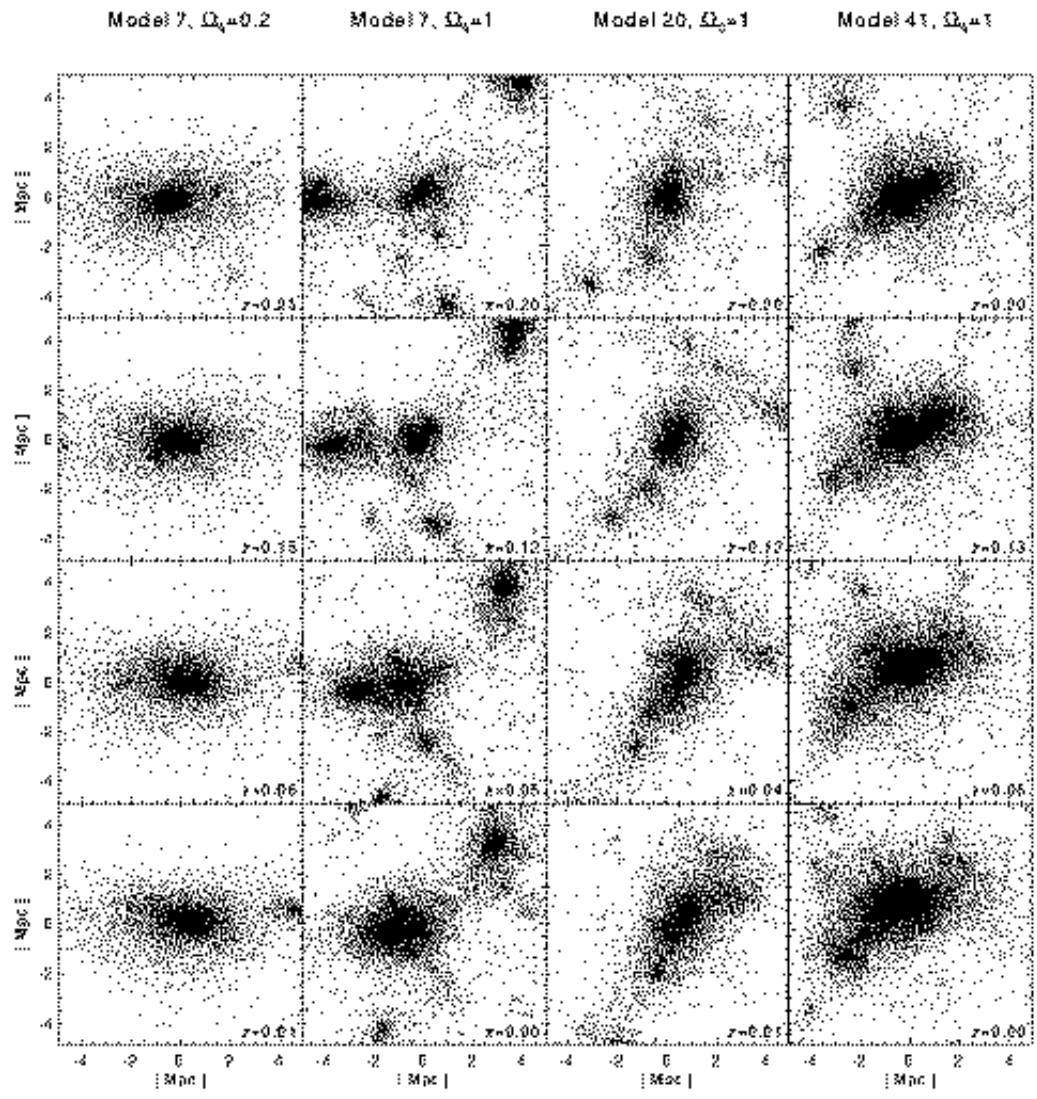
3.2 Four selected model clusters

We use cluster simulations from a model cluster catalogue constructed by van Kampen & Katgert (1996) for the $\Omega_0 = 1$ standard CDM scenario. They found a consistent value for σ_8 (the *r.m.s.* density fluctuation within spheres of $8h^{-1}\text{Mpc}$) which is used to normalise the density fluctuation spectrum. A match between models and data for the galaxy autocorrelation function, the richness distribution function, and the line-of-sight velocity dispersion favours $\sigma_8 \approx 0.4 - 0.5$. This is consistent with recent results of Eke et al. (1996), who find $\sigma_8 \approx 0.5$ for the same scenario. We therefore adopt a value of 0.5 for σ_8 . The Hubble parameter H_0 is set to $50 \text{ km s}^{-1} \text{ Mpc}^{-1}$ throughout this paper.

For this paper we selected cluster Models 7, 20 and 41 from the full catalogue. We also built the corresponding models for an $\Omega_0 = 0.2$ CDM scenario, i.e. we kept the same random numbers for the initial conditions but just changed Ω_0 . This low- Ω_0 variant of CDM was normalized according to the results of Eke et al. (1996), who find from the number density of clusters that σ_8 scales with Ω_0 as $0.5\Omega_0^{-0.47+0.10\Omega_0}$. Therefore, for $\Omega_0 = 0.2$ we are required to set $\sigma_8 \approx 1$, i.e. to the unbiased value. Here we only consider the $\Omega_0 = 0.2$ version of Model 7. These four models, with around 10^4 particles per cluster, form our basic simulation set. We re-simulated all models from $z = 0.2$ up to the present epoch, and saved the particle data frequently to get a finer timeslicing than the original run. Furthermore, since we do not expect to see any new galaxies forming within the clusters at these low redshifts, we switched off the galaxy formation algorithm in order to simplify the book-keeping of particle numbers. In Fig. 2 we show four epochs of the time evolution of the selected four cluster models. This figure will be discussed in more detail in Section 5.1.

3.3 Resolution and two-body relaxation

The resolution of an N-body model is primarily set by the particle softening that has to be employed in order to reduce numerical two-body relaxation effects, i.e., to make the simulations as collisionless as possible. However, one still wants to model the density distribution with sufficiently high spatial resolution, so a trade-off between resolution and acceptable two-body relaxation has to be made. With this in mind, previous experience (van Kampen 1995) shows that a Plummer softening parameter of 40 kpc is a good choice for the dark matter particles. This corresponds to 1/25th of the initial mean particle separation, which is well within the range of values argued for by various other users of treecodes (e.g. Bouchet & Hernquist 1988; Barnes & Hut 1989; Hernquist & Barnes 1990; Dyer & Ip 1993). The softening of the *galaxy particles* depends on the half-mass radius of the original simulation group that was ‘transformed’ into a galaxy. Typical values fall in the range 20–50 kpc (see van Kampen 1996), which are also well within the range usually found for treecodes. However, galaxy particles can have masses up to two hundred times larger than that of the dark matter particles, which means that an interaction between a galaxy and a dark matter particle can cause a significant change in the velocity of the latter, despite the softening. On the other hand, the dark matter particles outnumber the galaxies 50 to 1. For the models studied in this paper the collective con-



tribution of galaxy particles to the relaxation of dark matter particles is up to five times that of the dark matter particles themselves (van Kampen 1996). However, for our models the corresponding relaxation time is still at least 6 times t_0 , the present age of the universe ($30t_0$ if we had just dark matter particles). For the chosen value of H_0 here, $t_0 \sim 1 \times 10^{10}$ yr. So while simultaneously retaining the collisionless nature of the simulation, we do need to bear in mind the differing contributions of the two components to the deflection of particle orbits.

4 CONSTRUCTING THE DF FOR GALAXY CLUSTER MODELS

Since the positions, velocities and energies of all the particles that constitute a cluster model grown in a cosmological N-body simulation are known, the distributions $h(\mathcal{E})$, $g(\mathcal{E})$ and $f(\mathcal{E})$ can be evaluated. In this section we describe the exact procedure followed to construct the DF for such a system.

For any given snapshot we first compute the centre of mass enclosed by clumps within a 12 Mpc shell and then recompute this within 2 Mpc around the most massive clump. Any systematic velocity with respect to the centre of mass is subtracted, which is equivalent to ensuring that the main clump defines the origin of phase-space. This in turn defines $\Psi(r)$ and \mathbf{v} , and thus \mathcal{E} through eq. (4). It is then straightforward to compute the differential energy distribution $h(\mathcal{E})$ as a histogram of the distribution of mass in bins of energy.

Whereas no assumptions regarding the geometry of the configuration enter the definition of $h(\mathcal{E})$, our aim of computing $f(\mathcal{E})$ necessarily incorporates the approximation of spherical symmetry. This occurs during the computation of $g(\mathcal{E})$ wherein although the exact potential for the particles is known precisely from the simulation, a spherically averaged value is used. The potential for Model 20 ($z = 0$) is shown in Fig. 3a. Rather than simply averaging the observed potential in each radial bin we fit an analytical form to the data points. Overplotted are fits to the Hernquist potential and the NFW potential. Both yield acceptable fits for the spherically averaged potential and density profile (Fig. 3b) within the virial radius. Note here from Fig. 3a that at the virial radius the potential is roughly half of its central value, which is still deep inside the potential well. Therefore matter from the infall region does not significantly influence the dynamics within the virialized region.

Examining several morphologically distinct cluster models we find that the quality of the fit to these analytic models depends crucially on the degree of substructure in the cluster which shows up as the spread in $\Psi(r)$ in Fig. 3a. The fits get progressively worse for clumpy models since for these the centre of the potential is not well-determined and the shape departs maximally from sphericity even within the virial radius.

The advantage of using the Hernquist potential fit is that the modified density of states,

$$g(\mathcal{E}) = 16\pi^2 \int_0^{r_m(\mathcal{E})} \sqrt{2\left(\frac{\Psi_0}{1+\frac{r}{s}} - \mathcal{E}\right)} r^2 dr, \quad (25)$$

can be computed analytically (see Appendix A). The disadvantage of using such a fit to a given restricted form is in fact rather small since a much more severe limitation is

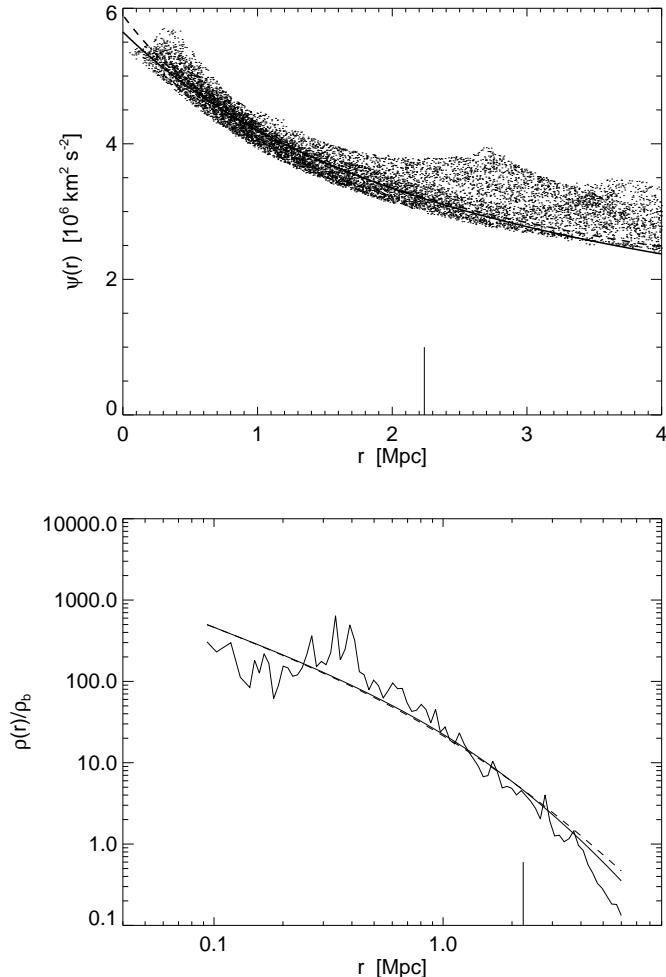


Figure 3. The density profile and potential for Model 20 for the snapshot taken at $z = 0$ are plotted above. In the top panel (a) the points are the exact potential from the simulation and overlotted are the fit to the Hernquist profile (solid curve) [with fit parameters: $\Psi_0 = 5.6 \times 10^6 \text{ km}^2 \text{ s}^{-2}$; $s = 2.89 \text{ Mpc}$] and the NFW profile (dashed curve) [with fit parameters $\Psi_{\text{NFW}} = 6.44 \times 10^6 \text{ km}^2 \text{ s}^{-2}$; $s = 1.09 \text{ Mpc}$]. The lower panel (b) shows the spherically averaged density profile overlaid with the Hernquist model (solid curve) [with fit parameters: $\rho_0 = 50.70 \rho_b$; $s = 3.18 \text{ Mpc}$] and NFW model (dashed curve) [with fit parameters: $\rho_0 = 51.33 \rho_b$; $s = 1.82 \text{ Mpc}$]. In both panels the large tick mark on the x-axis marks the value of $r_{180} = r_{\text{max}} = 2.24 \text{ Mpc}$.

our initial assumption of spherical symmetry. For these reasons we have used the Hernquist fit (Cole & Lacey 1996) in our computations of the density of states. However, we must emphasize here that the entire procedure is independent of the precise choice of functional form for the fitted potential and we only use the Hernquist fit to the potential for convenience and because it does provide an elegant analytic form for $g(\mathcal{E})$.

The distribution function $f(\mathcal{E})$ is then constructed using the definition in equation (9). For the snapshot at $z = 0$ for Model 20, the computed $h(\mathcal{E})$, $g(\mathcal{E})$ and $f(\mathcal{E})$ are shown in Fig. 4. From this figure we see that $h(\mathcal{E})$ (top panel) has a broad distribution and has a small fraction of positive energy particles. The effect of our prescription for truncating the

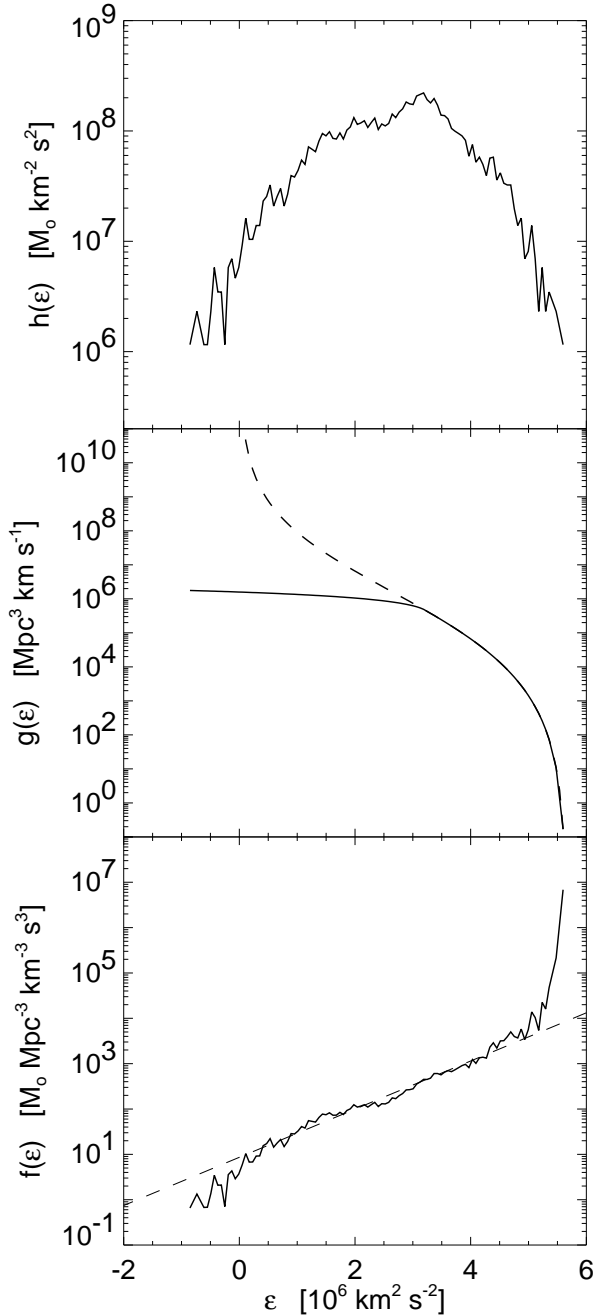


Figure 4. The computed quantities for a slice of Model 20 ($\Omega_0 = 1$) at $z = 0$. The top panel shows the differential energy distribution $h(\mathcal{E})$ for particles inside the virial radius, plotted as a histogram in energy bins. The middle panel shows the density of states in each energy hypersurface $g(\mathcal{E})$. The dashed curve is the usual equilibrium definition of $g(\mathcal{E})$ (eq. 8) computed analytically using a Hernquist fit to the potential, which diverges at $\mathcal{E} = 0$ (cf. Fig. 3). The solid curve uses equation (25), i.e., with the devised truncation (19) prescription presented in Fig. 1. Finally, the bottom panel shows the distribution function $f(\mathcal{E})$ obtained by dividing $h(\mathcal{E})$ (top panel) with the modified $g(\mathcal{E})$ (solid curve in middle panel). The overplotted dashed line is the best particle-number weighted exponential fit to the curve.

system in the computation of $g(\mathcal{E})$ is shown in the middle panel, where the solid curve corresponds to the restricted $g(\mathcal{E})$ and the dashed curve shows the asymptotic behavior (divergent) in the vicinity of $\mathcal{E} = 0$. In the bottom panel, we see that the computed $f(\mathcal{E})$ is remarkably well-fit by an exponential function of the form $f(\mathcal{E}) = f_0 e^{-\mathcal{E}/\sigma_{\text{fit}}^2}$ (the overplotted dashed curve), in the region dominated by the tightly bound particles, except in the deep potential region. We discuss this effect further in Section 5.2.

Defining the dimensionless central potential,

$$W_0 = \frac{\Psi_0}{\sigma_{\text{fit}}^2}, \quad (26)$$

the equivalent *r.m.s.* 1D velocity dispersion $\sigma_{1D}(r)$ can be computed analytically given σ_{fit} and Ψ_0 by comparing with the King model (the lowered exponential, see Binney & Tremaine (1987) for details) which also has an exponential $f(\mathcal{E})$,

$$\sigma_f^2 \equiv \frac{1}{3} \langle v^2 \rangle = 1 - \frac{8}{15\sqrt{\pi}} \delta W_0^{-5/2} \sigma_{\text{fit}}^2, \quad (27)$$

with

$$\delta = \exp(W_0) \text{erf}(\sqrt{W_0}) - \sqrt{\frac{4W_0}{\pi}} \left(1 + \frac{2W_0}{3}\right). \quad (28)$$

The velocity dispersion computed from the fit to the constructed isotropic distribution function $f(\mathcal{E})$ agrees well (to within 5%) with the mean 1D velocity dispersion inside r_{180} computed directly from the simulation.

The DF can also be compared to a characteristic phase-space density

$$\bar{f} \equiv \frac{3}{8\pi^{5/2}} \frac{M(r_{\text{max}})}{r_{\text{max}}^3 \sigma_{1D}^3}, \quad (29)$$

motivated by the expression for the central phase-space density of the isothermal sphere, $f_c = (2\pi)^{-3/2} \rho_c \sigma^{-3}$. For Model 20, which has $M(r_{\text{max}}) = 5.87 \times 10^{14} M_\odot$, $r_{\text{max}} = 2.24$ Mpc and $\sigma_{1D} = 970$ km s $^{-1}$, we find $\bar{f} \approx 1200 M_\odot \text{Mpc}^{-3} \text{km}^{-3} \text{s}^3$. This fits in nicely with the distribution function $f(\mathcal{E})$ as plotted in Fig. 4. These comparisons clearly demonstrate that the entire procedure produces sensible results, both quantitatively and qualitatively.

To compute the anisotropic distribution function $f(\mathcal{E}, L)$ we use the definitions in equations (12), (23) and (24), once again with $r_{\text{max}} = r_{180}$, the expected virial radius. The surface plots for $h(\mathcal{E}, L)$, $g(\mathcal{E}, L)$ and $f(\mathcal{E}, L)$ are shown in Fig. 5. The $h(\mathcal{E}, L)$ distribution has a coherent peak at low values of angular momentum and energy. Unlike Voglis (1994), who analysed galaxies, we do not find a differentiated core and halo population for a galaxy cluster on equivalent scales, although there exists a small fraction of positive energy particles. The anisotropic DF is sharply peaked and falls off to zero for large \mathcal{E} , similar to $f(\mathcal{E})$. To conclude this section, we have demonstrated that DFs can be constructed self-consistently for N-body model clusters and that sensible results are obtained.

5 RESULTS

In this section we analyse the dynamical states of the model clusters (restricted to the virialized central region by construction) using the time evolution of the DF in conjunction

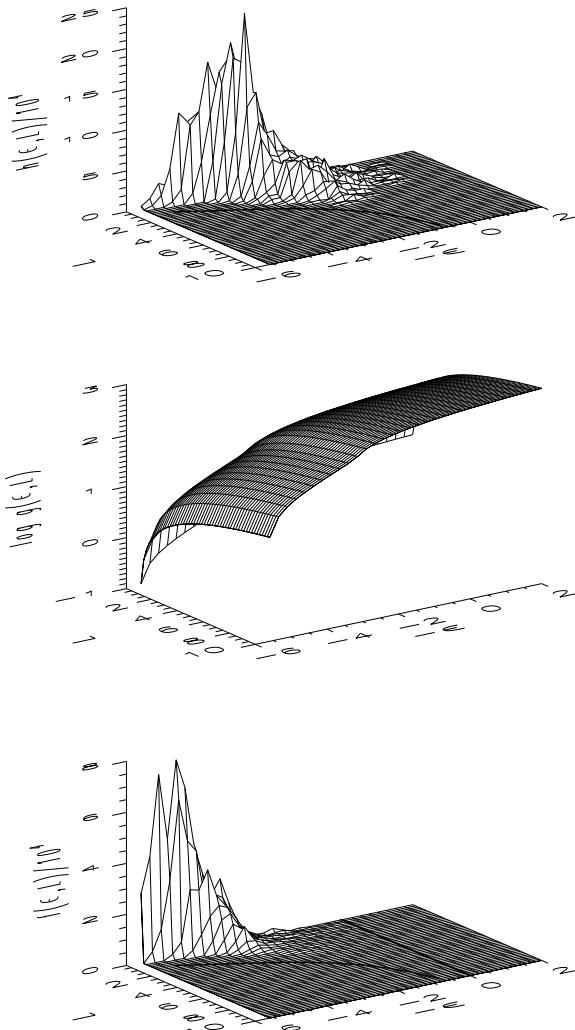


Figure 5. The anisotropic distribution function. The figures show (from the top to bottom) the differential distribution $h(\mathcal{E}, L)$, the modified density of states $g(\mathcal{E}, L)$ and the constructed distribution function $f(\mathcal{E}, L)$ for Model 20. Here $h(\mathcal{E}, L)$ is in units of $M_{\odot} \text{Mpc}^{-1} \text{km}^{-3} \text{s}^3$, $g(\mathcal{E}, L)$ in units of $M_{\odot} \text{Mpc}^2$ and $f(\mathcal{E}, L)$ in units of $M_{\odot} \text{Mpc}^{-3} \text{km}^{-3} \text{s}^3$. Here \mathcal{E} is in units of $10^6 \text{km}^2 \text{s}^{-2}$ and L in units of Mpc km s^{-1} .

with other physically interesting quantities. Before embarking on a discussion of the various distribution functions, it is instructive to briefly outline the evolution as seen in the N-body simulations for the studied models shown in Fig. 2.

Model 7 evolving in the $\Omega_0 = 0.2$ universe, is relatively isolated and its evolution is being traced during a passively evolving phase. Model 7 ($\Omega_0 = 1$) has a significant amount of substructure and undergoes a violent merging event at the present epoch, while Model 41, which is a significantly

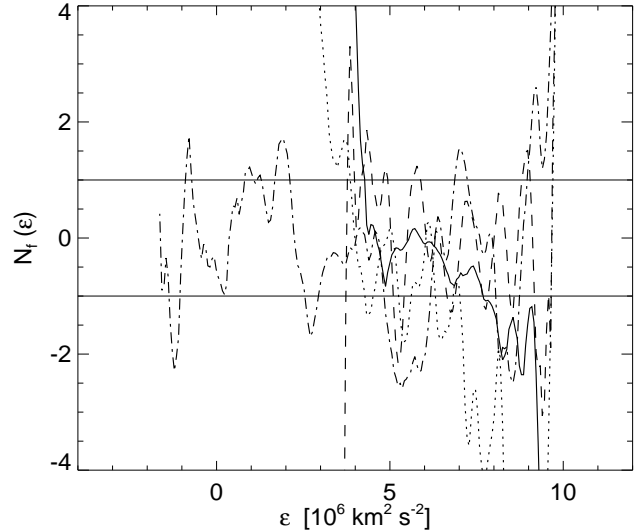


Figure 6. The fractional change in $f(\mathcal{E})$, $N_f(\mathcal{E})$ during a typical dynamical time for the four clusters computed at $z = 0$ are plotted above. The solid curve corresponds to Model 7 (evolved in an $\Omega_0 = 0.2$ universe), the dotted curve to Model 7, the dashed curve to Model 20 and the dot-dashed curve to Model 41 (all three evolved in an $\Omega_0 = 1.0$ model). The horizontal lines correspond to $N_f = 1$ and -1 .

more massive cluster, is being followed during one of its more quiet evolutionary stages.

The three $\Omega_0 = 1$ models are typical for the standard CDM scenario in the sense that a cluster does not form from a single collapse but rather from a heterogeneous collapse, typically from two or more diffuse sub-clumps that grow individually and merge to form the final cluster. Before and after these mergers the cluster grows by accreting material along several filaments, which join at the position of the cluster. This ‘secondary’ infall proceeds in a somewhat lumpy fashion. The complex aggregation process implies that present-day cluster cores are often obscured by surrounding clumps. The fact that these clumps are falling towards the cluster makes it hard to distinguish them when observing along the line of sight in redshift space. The $\Omega_0 = 0.2$ cluster model is also representative for its cosmology, in the sense that clusters form early in this scenario, show only little secondary infall, and few merging clumps. We therefore expect this model to be relatively close to equilibrium, even though small clumps are still falling in and the dynamical timescale is about a sixth of a Hubble time.

In the following subsections we briefly discuss what can be learnt from this new DF approach. The emphasis will be on demonstrating the usefulness and reliability of our construction of distribution functions, using the N-body models to illustrate the results. Detailed discussions of the dynamics of cluster formation and the cosmological implications using this approach are deferred to later papers.

5.1 Time scales and quasi-equilibrium

As anticipated in Sections 2.1 and 2.3, it is evident from the evolution plots in Figs. 7, 8 and 9, that in general, even over relatively short time scales (compared to the Hubble time), the dynamical state changes perceptibly, thus validating the

quasi-equilibrium approach of treating the system as one evolving over two characteristic but disparate time-scales.

To test the assumption that clusters are indeed in a quasi-equilibrium state at least in the interim between major merger events, we calculate the fractional change in $f(\mathcal{E})$ during one dynamical time $t_{\text{dyn}} \equiv \sqrt{3\pi/16G\rho}$ (Binney & Tremaine 1987), which is equal to $0.25t_0$ (for the flat model), as $\rho = \rho_{180} = 180\rho_b$ for the virialized region under study (by definition). At $z = 0$ we compute the dimensionless quantity $N_f(\mathcal{E})$ defined to be a measure of the stationarity,

$$N_f(\mathcal{E}) \equiv t_{\text{dyn}} \left(\frac{df}{dt} \cdot \frac{1}{f} \right), \quad (30)$$

plotted in Fig. 6. In order to get a quantitative measure for the stationarity of $f(\mathcal{E})$, we calculate the $h(\mathcal{E})$ -weighted averages of $N_f(\mathcal{E})$ for all four models and hence define the ‘stationarity index’ n_f as,

$$n_f \equiv \frac{\int |N_f(\mathcal{E})| h(\mathcal{E}) d\mathcal{E}}{M}, \quad (31)$$

where M is the total mass enclosed within r_{180} for the system. The values of n_f that we find are: 0.32, 3.3, 3.7, and 0.96 for Model 7 ($\Omega_0 = 0.2$), 7 ($\Omega_0 = 1$), 20, and 41 respectively. We interpret this as follows: only Model 7 for the $\Omega_0 = 0.2$ case can really be considered to be in quasi-equilibrium, with clear skewing evolution of $f(\mathcal{E})$, while the same model within an $\Omega_0 = 1$ universe, where it is undergoing a major merger, and Model 20 are furthest from an equilibrium state. Model 41 is a ‘critical’ case: there certainly is on-going secondary infall, but the cluster is almost massive enough for the virialized region to remain in quasi-equilibrium. Therefore, we roughly delineate three distinct regimes on the basis of the values of the ‘stationarity’ index n_f : $n_f < 1$ corresponds to the regime where the quasi-equilibrium description is an adequate one, $n_f = 1$ to the critical case and $n_f > 1$ to the case when the system has departed from quasi-equilibrium while recuperating from a merger.

5.2 Signatures of substructure

As mentioned in Section 4 there appears to be a central peak in $f(\mathcal{E})$ for most of the models. The peak is particularly marked when there is significant substructure inside the studied region. We therefore associate this peak with infalling sub-clumps outside the cluster core which already have a deep ‘local’ central potential, but contain an insignificant fraction of the mass of the system. Indeed, the effect is not seen in $h(\mathcal{E})$ confirming the above picture. The central peaks in $f(\mathcal{E})$ are thus partially an artifact of the assumption of spherical symmetry of the potential, but are also a signature of transient substructure. Once the clumps are incorporated or fall in to the centre of the cluster, the peak disappears.

The radial profile for the velocity anisotropy parameter,

$$\beta(r) \equiv 1 - \frac{\sigma_\theta^2(r)}{\sigma_r^2(r)}, \quad (32)$$

is correlated to the presence of substructure (see Fig. 2). In the absence of significant sub-clustering the velocity distribution is found to be roughly isotropic but erratic ($\beta \approx 0$) and for quiescent evolution $\beta > 0$, indicating the presence

of primarily radial orbits, which are most likely to originate in the infall region.

The presence of substructure in the cluster models being progressively subsumed into the main clump can be seen in the (significant) evolution of the 1D velocity dispersion profiles as well. For example, consequent to a merger the mean value increases as shown in the top left panel of Fig. 8. Furthermore, the overall shape seems to be well correlated with substructure and secondary infall. This promises to be one of the important applications of the DF formalism.

5.3 Evolution in the density profiles

Comparatively little systematic evolution is seen in the density profiles, aside from the progressive worsening of the fits to the analytic form occurring due to the presence of sub-clumps causing significant departures from sphericity, and small changes in the value of the central density. Density profiles seem to be set up rather early in the evolutionary history of the cluster.

5.4 The central potential and degree of central condensation

The dimensionless depth of the potential, W_0 as defined in equation (26), is a measure of the central concentration of the system. For the models studied, we find $W_0 \approx 7$ for the flat models and $W_0 \approx 10.5$ for the open model. This is comparable to what is found for elliptical galaxies, where $8 \lesssim W_0 \lesssim 11$ (Hjorth & Madsen 1995), and uncollapsed globular clusters for which $W_0 \lesssim 10$ (eg. Binney & Tremaine 1987). Clusters evolving in an Einstein-de Sitter universe have comparatively shallower central potentials since the system is constantly disturbed by infalling sub-clumps and is hence unable to build up a concentrated core in the elapsed time. By contrast, a cluster evolving in an open universe is comparatively more homogeneous and relatively undisturbed. It evolves quiescently essentially due to the fact that dark matter particles are allowed to plunge down into the centre on radial orbits (as evidenced by $\beta > 0$ seen in the middle left panel of Fig. 7) hence building up to high central densities.

The observed trends in the central concentration can also be potentially related to features of the initial conditions by estimating the characteristic phase-space density \bar{f} . The typical maximum phase-space density is about 100 times larger than this characteristic value, similar to what has been found for elliptical galaxies. Since the maximum phase-space density cannot increase during collisionless evolution for an isolated system (Tremaine, Hénon, & Lynden-Bell 1986), the computed value of \bar{f} allows us to understand the relative efficiency required of any relaxation process, given characteristic time-scales of mediation, in order to produce the present configuration from the inhomogeneous initial cosmological conditions from which a cluster first assembles.

5.5 Energy distribution

There is a clear difference between the differential energy distributions, $h(\mathcal{E})$, of the open and flat models. The energy dis-

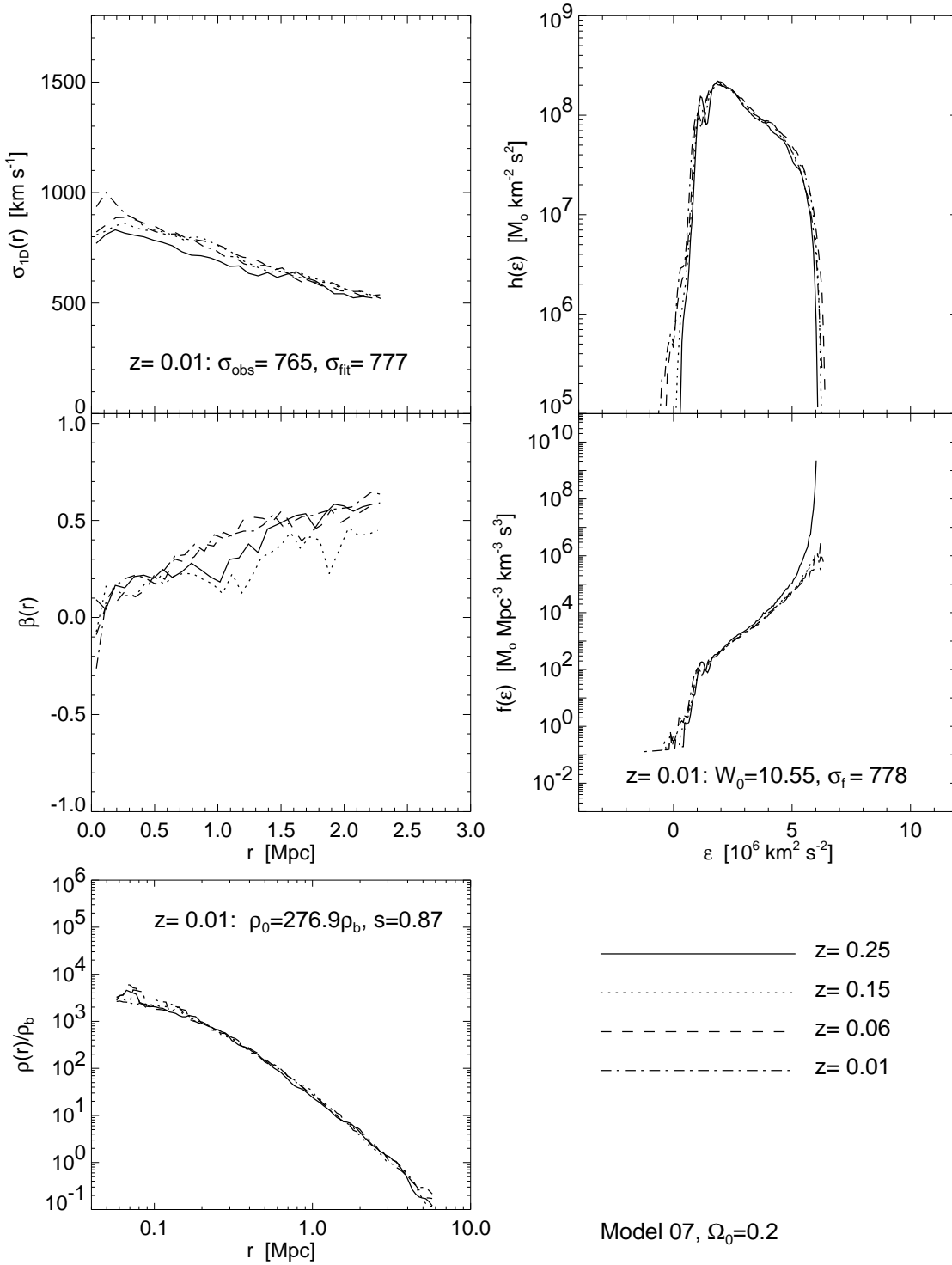


Figure 7. The evolution of computed quantities for a slice of Model 7 ($\Omega_0 = 0.2$) for four redshifts chosen to correspond to constant time intervals. As a function of physical radius, the left panel shows the measured one-dimensional velocity dispersion $\sigma_{1D}(r)$ (top), the anisotropy parameter $\beta(r)$ (as defined in eq. 32) (middle), and the density $\rho(r)$ relative to the background density ρ_b (bottom). In the right panel the differential energy distribution $h(\mathcal{E})$ (top) and the computed isotropic distribution function $f(\mathcal{E})$ (middle) are plotted as a function of the binding energy per unit mass \mathcal{E} .

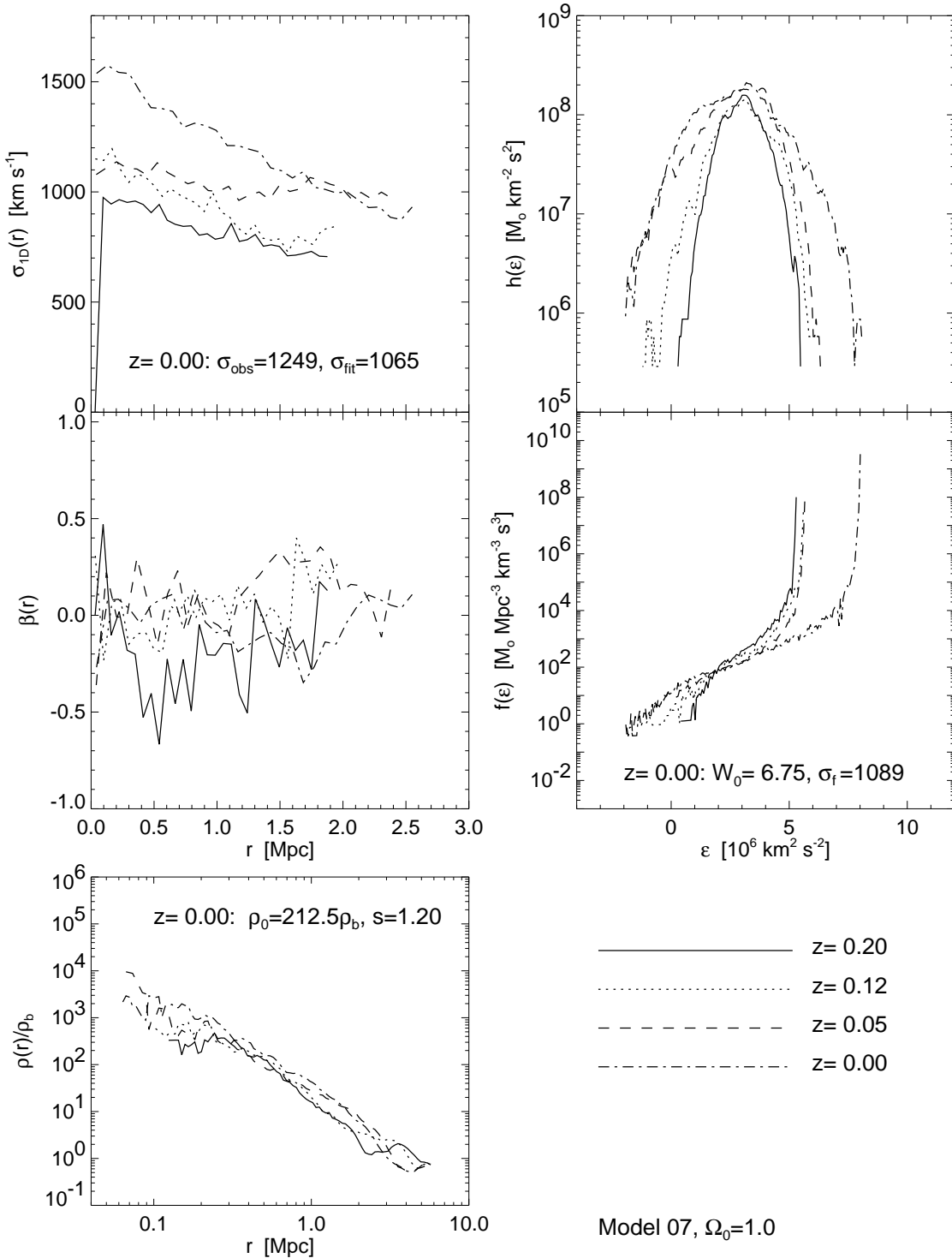


Figure 8. Same as Fig. 7 for Model 7 within an $\Omega_0 = 1$ Universe.

tribution for the open model (Fig. 7) is very similar to that of elliptical galaxies where a ‘negative temperature’ exponential function, cut-off close to the escape energy ($\mathcal{E} = 0$), provides a good fit the $h(\mathcal{E})$ (Binney 1982), i.e., most of the particles are loosely bound. By contrast, the energy distribution of the flat models are better approximated by gaus-

sians with a tail of positive-energy particles. The advantage of our adapted DF formalism is that it allows the inclusion of positive energy particles as well. For the galaxy cluster models evolved in a flat universe we find that the particles with positive energies that are located preferentially in the centre of the cluster, despite the deep potential well. Energy

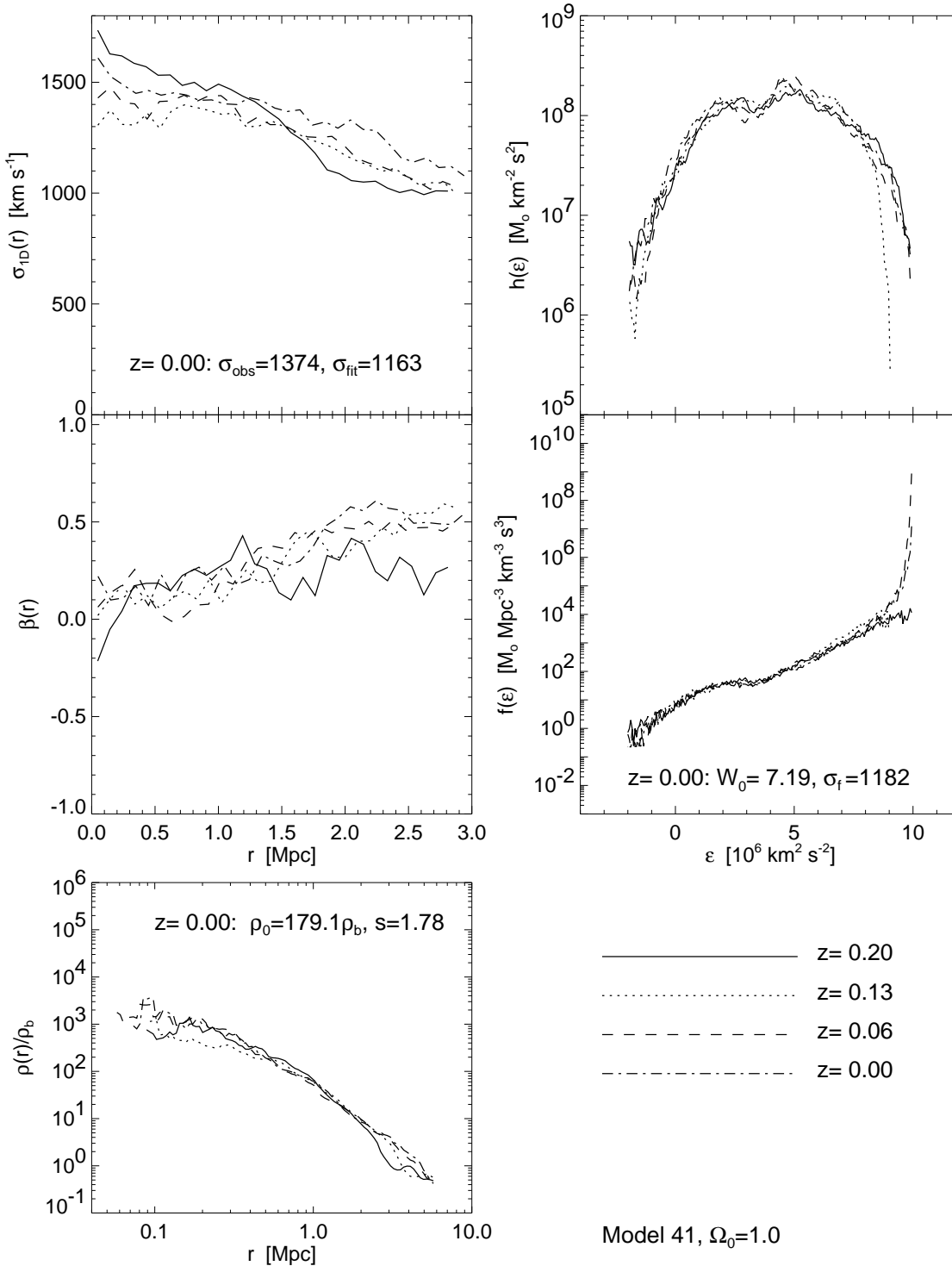


Figure 9. Same as Fig. 7 for Model 41 ($\Omega_0 = 1$).

exchange due to violent merger events as seen in Model 7 for $\Omega_0 = 1.0$, for instance, are a potential source for generating these unbound particles, as we clearly see a significant fraction of them just before and during a merger. We also detect simultaneously a surge in the maximum value of \mathcal{E} , indicating significant energy diffusion. We hope to address

this issue in the context of examining the relaxation process in more detail in a future paper.

6 SUMMARY AND CONCLUSIONS

In this paper we have applied an adapted version of the distribution function formalism of equilibrium stellar dynamics to numerical models of clusters of galaxies. Clusters are generally not in equilibrium as on-going secondary infall and the relatively long dynamical time-scale prevent them from reaching an equilibrium configuration. However, as evidenced from observations of clusters, this deviation from equilibrium is not expected to be too severe, at least within the finite central virialized region, and so a quasi-equilibrium description can be formulated enabling the construction of the distribution function for the N-body cluster models.

Isotropic $f(\mathcal{E})$ and anisotropic $f(\mathcal{E}, L)$ distribution functions can be computed using the differential energy distribution and the density of available states in phase space for the system. The accessible phase space however, needs to be restricted in a physically meaningful and self-consistent fashion. We invoke the finite elapsed time since formation and space available as providing a natural way to limit phase space. We argue that this prescription can be suitably applied when the analysis is restricted to the virialized region, which is defined by $r \leq r_{180}$. This is motivated by the fact that the particles that once enter and get bound within this region are not likely to leave. Even particles that do become unbound due to energy-exchange processes are likely to lose energy fairly rapidly in the dense cluster environment on very short time-scales, i.e., their occupancy of states in phase space is automatically limited by the fact that particles are expected to change energy again within a relatively short time. It is precisely the existence of these two disparate time scales (the long dynamical time scale and the short characteristic time scale for energy exchange) which implies that the evolution of the system can be effectively decoupled into ‘fast’ and ‘slow’ components and hence allows the description of quasi-equilibrium states somewhat within the equilibrium formalism. In the anisotropic case it is additionally assumed that $g(\mathcal{E}, L)$ is separable.

We show that this construction can be successfully accomplished for N-body cluster models taken from a large sample of models for the standard CDM cosmological scenario, and that the constructed DFs do show similarities to equilibrium ones. The velocity dispersion as obtained from an exponential fit to $f(\mathcal{E})$ agrees well with that obtained directly from the particle distribution in the N-body simulation (agrees to within 5 % typically). This is not only true for specific redshift slices, but also during the course of evolution. The only exceptions are during strong merger events, whence the difference can be a few hundred km s^{-1} . The characteristic phase-space density, calculated from global properties of the particle distribution in the simulation and from the computed DF also agree well.

Furthermore, we show by following the time variation of the DFs that they are good tracers of dynamical events like cluster mergers and infall of clumps. There is notable evolution with redshift for most models, indicating on-going dynamical evolution. The exception is the cluster model simulated in an $\Omega_0 = 0.2$ CDM universe, which shows only mild evolution and can be said to be in quasi-equilibrium. It is also the only model to show a linear rise of the velocity anisotropy parameter β from zero in the centre of the cluster to about 0.5 at r_{180} . This cluster bears the closest resem-

blance to an elliptical galaxy, further demonstrated by the shape of $h(\mathcal{E})$ and the degree of central concentration which is well within the range typically estimated for ellipticals. We also find that the density profiles within the virialized region show practically no evolution and seem to be set up quite early in the dynamical history.

As to the possibilities of using the constructed DF to describe the dynamical state of a galaxy cluster, it can clearly distinguish the merging clusters from the quiet ones, as well as the ones dominated by secondary infall. The evolution of the DF, even over a relatively short time, reveals the on-going kinematic activity. The comparison of global properties like the velocity dispersion as obtained from a fit to $f(\mathcal{E})$ to those calculated directly from the simulation provide a new indicator to establish whether the cluster is close to equilibrium.

In a recent study of the evolution of cluster-scale dark halos, Tormen, Bouchet, & White (1996) also characterize the halo formation process as being composed of alternating merging and relaxation phases. The general picture that emerges from our analysis is one of clusters evolving quiescently with on-going collective energy exchange (which we define as quasi-equilibrium states) punctuated by violent merging phases followed by fairly brief, but yet well-defined recovery phases. During the passively evolving phases, we find that the DF $f(\mathcal{E})$ is well-approximated by an exponential and significant deviations occur only during the merging and recouping phases. In this treatment, we have not quantified the frequency or nature of energy exchange processes, aside from the observation that they do indeed occur. Besides possibly allowing a better understanding of the physics of energy exchange, this approach also potentially affords new discriminants of the underlying cosmological model.

In conclusion, we have shown that distribution functions can be successfully constructed for the dark matter component of evolving, non-isolated clusters of galaxies grown in N-body simulations. The necessary machinery is thus in place for future work in which we hope to address the use of distribution functions as a new probe of cluster dynamics and evolution, fundamental cosmological parameters, and the possible origin of ‘universal’ cluster density profiles.

7 ACKNOWLEDGMENTS

PN acknowledges Martin Rees and Donald Lynden-Bell for encouragement and insightful discussions during the course of this work. PN and JH thank John Peacock and the ROE for hospitality where a portion of this work was done. PN acknowledges financial support from the Isaac Newton Studentship and Trinity College, Cambridge; JH from the Danish Natural Science Research Council (SNF) and EvK the receipt of an EC HCM Research Fellowship. We acknowledge useful discussions with Bernard Jones, Steinn Sigurdsson, Simon White and Tim de Zeeuw.

APPENDIX A: TRUNCATED DENSITIES OF STATE FOR VARIOUS POTENTIALS

For the Hernquist (1990) potential used in this paper,

$$\Psi(r) = \frac{\Psi_0}{1 + \frac{r}{s}}. \quad (\text{A1})$$

where s is a characteristic scale radius, the truncated density of states can be expressed analytically as,

$$\begin{aligned} \frac{g(\mathcal{E})}{16\pi^2} &= -\frac{\sqrt{\Psi_0 - \mathcal{E}} (8\mathcal{E}^2 + 10\mathcal{E}\Psi_0 - 3\Psi_0^2) s^3}{12\sqrt{2}\mathcal{E}^2} \\ &+ \frac{A(8\mathcal{E}^2(r_m^2 + s^2 - r_m s) + 10\mathcal{E}\Psi_0 s^2 - 3\Psi_0^2 s^2 - 2\mathcal{E}\Psi_0 r_m s)(r_m + s)}{12\sqrt{2}\mathcal{E}^2} \\ &+ \frac{\Psi_0(8\mathcal{E}^2 - 4\mathcal{E}\Psi_0 + \Psi_0^2) s^3}{8\sqrt{2}\mathcal{E}^{5/2}} \left[\tan^{-1}\left(\frac{\Psi_0 - 2\mathcal{E}}{2\sqrt{\mathcal{E}}\sqrt{\Psi_0 - \mathcal{E}}}\right) - \tan^{-1}\left(\frac{A(2\mathcal{E}r_m + 2\mathcal{E}s - \Psi_0 s)}{2\sqrt{\mathcal{E}}(\mathcal{E}r_m + \mathcal{E}s - \Psi_0 s)}\right) \right] \end{aligned} \quad (\text{A2})$$

for $\mathcal{E} > 0$ and

$$\begin{aligned} \frac{g(\mathcal{E})}{16\pi^2} &= -\frac{\sqrt{\Psi_0 - \mathcal{E}} (8\mathcal{E}^2 + 10\mathcal{E}\Psi_0 - 3\Psi_0^2) s^3}{12\sqrt{2}\mathcal{E}^2} \\ &+ \frac{A(8\mathcal{E}^2(r_m^2 + s^2 - r_m s) + 10\mathcal{E}\Psi_0 s^2 - 3\Psi_0^2 s^2 - 2\mathcal{E}\Psi_0 r_m s)(r_m + s)}{12\sqrt{2}\mathcal{E}^2} \\ &- \frac{\Psi_0(8\mathcal{E}^2 - 4\mathcal{E}\Psi_0 + \Psi_0^2) s^3}{8\sqrt{2}(-\mathcal{E})^{5/2}} \left[\ln(2s(\sqrt{\Psi_0 - \mathcal{E}}\sqrt{-\mathcal{E}} - \mathcal{E}) + \Psi_0 s) - \ln(2(r_m + s)(A\sqrt{-\mathcal{E}} - \mathcal{E}) + \Psi_0 s) \right] \end{aligned} \quad (\text{A3})$$

for $\mathcal{E} < 0$. In these expressions,

$$A = \sqrt{\Psi_0 \frac{s}{r_m + s} - \mathcal{E}}. \quad (\text{A4})$$

Alternate popular potentials do not completely reduce to analytic expressions. For the NFW potential (Navarro, Frenk, & White 1996),

$$\Psi(r) = \frac{\Psi_{\text{NFW}} s}{r} \ln\left(1 + \frac{r}{s}\right), \quad (\text{A5})$$

the truncated density of states is

$$\frac{g(\mathcal{E})}{16\pi^2} = \frac{2}{\sqrt{5}} \int_0^{r_m} \frac{dr r^{\frac{5}{2}} (\mathcal{E} - \Psi_{\text{NFW}} \frac{s}{r+s})}{\sqrt{\Psi_{\text{NFW}} s \ln(1 + \frac{r}{s}) - r\mathcal{E}}} + \frac{2\sqrt{2}}{5} r_m^{5/2} \sqrt{\Psi_{\text{NFW}} s \ln(1 + \frac{r}{s}) - r_m \mathcal{E}}. \quad (\text{A6})$$

For the Jaffe model (Jaffe 1983),

$$\Psi(r) = \Psi_J \ln\left(1 + \frac{r_J}{r}\right), \quad (\text{A7})$$

the truncated density of states is

$$\frac{g(\mathcal{E})}{16\pi^2} = \frac{\Psi_J r_J}{3\sqrt{2}} \int_0^{r_m} dr \frac{r^2}{(r + r_J) \sqrt{\Psi_J \ln(1 + \frac{r_J}{r}) - \mathcal{E}}} + \frac{\sqrt{2}}{3} r_m^3 \sqrt{\Psi_J \ln(1 + \frac{r_J}{r_m}) - \mathcal{E}}. \quad (\text{A8})$$

For the singular isothermal sphere (Binney & Tremaine 1987),

$$\Psi(r) = \Psi_I \ln\left(\frac{1}{r}\right), \quad (\text{A9})$$

the truncated density of states is

$$\frac{g(\mathcal{E})}{16\pi^2} = \frac{\Psi_I}{3\sqrt{2}} \int_0^{r_m} dr \frac{r^2}{\sqrt{\Psi_I \ln(\frac{1}{r}) - \mathcal{E}}} + \frac{\sqrt{2}}{3} r_m^3 \sqrt{\Psi_I \ln(\frac{1}{r_m}) - \mathcal{E}}. \quad (\text{A10})$$

REFERENCES

- Barnes J., 1996, in Morrison H. L., Sarajedini A., eds, Formation of the Galactic Halo - Inside and Out. ASP Conf. Series, Dordrecht, p. 415
 Barnes J., Hut P., 1989, ApJS, 70, 389
 Binney J., 1982, MNRAS, 200, 951
 Binney J., Tremaine S., 1987, in Galactic Dynamics. Princeton Univ. Press, Princeton
 Bouchet F. R., Hernquist L., 1988, ApJS, 68, 521

- Carlberg R., 1995, private communication
Carlberg R., Lake G., Norman C., 1986, *ApJ*, 300, 1
Cen R., 1994, *ApJ*, 437, 12
Cen R., Gnedin N., Ostriker J., 1993, *ApJ*, 415, 423
Cole S., Lacey C., 1996, *MNRAS*, 281, 716
Crone M., Evrard A., Richstone D., 1994, *ApJ*, 434, 402
Dodds S. J., 1995, PhD thesis, University of Edinburgh
Dyer C. C., Ip P. S. S., 1993, *ApJ*, 409, 60
Eddington A., 1916, *MNRAS*, 76, 572
Eke V., Cole S., Frenk C. S., Navarro J. F., 1996, *MNRAS*, 281, 703
Goldreich P., 1984, *ApJ*, 281, 1
Hernquist L., 1990, *ApJ*, 356, 359
Hernquist L., Barnes J., 1990, *ApJ*, 349, 562
Hernquist L., Spergel D., Heyl J., 1993, *ApJ*, 416, 415
Hjorth J., Madsen J., 1991, *MNRAS*, 253, 703
Hjorth J., Madsen J., 1995, *ApJ*, 445, 55
Hoffman Y., Shaham J., 1985, *ApJ*, 297, 16
Jaffe W., 1983, *MNRAS*, 202, 995
Klypin A., Holtzmann J., Primack J., Regös E., 1993, *ApJ*, 416, 1
Londrillo P., Messina A., Stiavelli M., 1991, *MNRAS*, 250, 54
Lynden-Bell D., 1967, *MNRAS*, 136, 101
Lynden-Bell D., 1996, private communication
Merritt D., Tremaine S., Johnstone D., 1989, *MNRAS*, 236, 829
Navarro J., Frenk C. S., White S. D. M., 1996, *ApJ*, 462, 563
Navarro J., White S. D. M., 1994, *MNRAS*, 267, 401
Peebles J., 1980, in *The Large-Scale Structure of the Universe*. Princeton University Press, Princeton
Richstone D., Loeb A., Turner E., 1992, *ApJ*, 393, 477
Spergel D. N., Hernquist L., 1992, *ApJ*, 397, 75
Stiavelli M., Bertin G., 1987, *MNRAS*, 229, 61
Tormen G., Bouchet F., White S. D. M., 1996, *MNRAS* in press.
Tremaine S., 1987, in De Zeeuw T., ed, *Structure and Dynamics of Elliptical Galaxies*. IAU Symp. 127, Dordrecht, p. 367
Tremaine S., Hénon M., Lynden-Bell D., 1986, *MNRAS*, 219, 285
van Albada T., 1982, *MNRAS*, 201, 939
van de Weygaert R., Bertschinger E., 1996, *MNRAS*, 281, 84
van Kampen , Katgert P., 1996, preprint.
van Kampen E., 1995, *MNRAS*, 273, 295
van Kampen E., 1996, preprint, submitted to *MNRAS*
Voglis N., 1994, *MNRAS*, 267, 379
West M. J., Dekel A., Oemler A., 1987, *ApJ*, 316, 1
White S. D. M., 1996, in Lahav O., Terlevich E., Terlevich R., eds, *Gravitational Dynamics*. Cambridge Univ. Press, Cambridge, p. 121

This figure "evopicts.gif" is available in "gif" format from:

<http://arxiv.org/ps/astro-ph/9609049v2>